Phase-modulated ellipsometer using a Fourier transform infrared spectrometer for real time applications

A. Canillas,[a] E. Pascual,[a] and B. Drévillon
Laboratoire de Physique des Interfaces et des Couches Minces (UPR 258 du CNRS), Ecole Polytechnique, 91128 Palaiseau, France

(Received 9 December 1992; accepted for publication 5 May 1993)

A new Fourier transform infrared phase-modulated ellipsometer is presented. It combines the high frequency provided by a photoelastic modulator (37 kHz) with the low frequency of the Fourier transform infrared spectroscopy (<1 kHz), by means of a numerical data acquisition system. A full spectrum recording (from 900 to 4000 cm^{-1}) can be achieved in 2 s. Thus, it allows its adaptation for kinetic *in situ* studies. The optical setup and the data reduction procedure are presented. In particular, a self-consistent spectral calibration procedure is described in detail. The precision in Ψ and Δ increases from 0.3° to 0.02° when increasing the integration time from 2 to 760 s. The examples shown in this article illustrate the high sensitivity to identify and analyze the absorption vibration variations of ultrathin films (a few angstroms thick).

I. INTRODUCTION

Infrared (IR) ellipsometry has emerged recently as a powerful optical technique to characterize surfaces, interfaces, and thin films. The growing interest in the development of the ellipsometry in the IR comes, on the one hand, from the well-established performances of spectroscopic ellipsometry in the visible and near ultraviolet (UV), namely, high-sensitivity, noninvasive technique and the possibility of *in situ* and real time operations; on the other hand, from the fact that the high penetration depth of IR light makes easy the film bulk characterization. Moreover, IR ellipsometry presents two major advantages with respect to the conventional transmission IR spectroscopy: a high sensitivity that allows chemical bond identification on various substrates at the monolayer scale, together with the capability to determine, directly from the measured data, the complex dielectric function of the material under study.

The first spectroscopic IR ellipsometers were based on the use of grating monochromators with rotating polarizer (RPE),[1] analyzer (RAE)[2] or photoelastic modulator (PME).[3] The sensitivity of these instruments is limited by the weak detected signal intensity. In order to improve the sensitivity, the intensity provided by the IR source must be increased, as it has been recently shown with a phase-modulated IR ellipsometer (IRPME) that implements a cascade arc source (hot-argon plasma).[4–6] In order to combine ellipsometry advantages with the well-known advantages of Fourier transform (FT) spectroscopy,[7] the coupling of traditional ellipsometric arrangements on commercial FTIR spectrometers was proposed. Thus, FTIR ellipsometers based on the RAE configuration were realized.[8–10] These instruments incorporate conventional IR sources and present a remarkable sensitivity. However, they cannot be used for monitoring fast processes since spectra are obtained from almost three interferograms recorded at different fixed analyzer orientations. This experimental procedure is mainly due to the polarization frequency, produced by the rotation of a polarizer, at a 100–200 Hz scale that overlaps with the interferogram frequencies, usually less than 1 kHz. FTIR reflection absorption spectroscopy (FT-IRAS) can combine FTIR spectroscopy and phase modulation.[11] However, dealing only with one frequency of the detected signal, it cannot allow the complete ellipsometric measurements. An attempt of FTIR phase-modulated ellipsometry (FTPME) has been recently presented.[12] However, the Bessel function background produced in the spectra due to the achromicity of the photoelastic modulator is not removed. Moreover, a calibration procedure using known standards (ZnSe prism and Ge plate) is needed to improve the accuracy.[12]

This article presents a new and more general arrangement designed for real time applications, such as kinetic *in situ* studies.[13] The original part of the present apparatus is the data acquisition system, which is based on a digital microprocessor (DSP) well adapted to the fast Fourier transform (FFT). This allows the high frequency of the photoelastic modulator (37 kHz) and the low frequency of the interferogram (<1 kHz) to be combined without overlap. A simple self-consistent calibration procedure will be also described. This calibration allows the removal of the Bessel function background and can be easily automatized.

This article is organized as follows. In Sec. II the basic mathematical and optical formalism necessary to describe FTPME are presented. Section III describes the experimental setup and the data acquisition system. The calibration procedure is presented in Sec. IV. Finally, Sec. V is devoted to the illustration of the performance of the ellipsometer. The first example deals with the presence of the very thin (20 Å) native oxide film on the crystalline silicon(c-Si) surface. The second example is related to the crystallization of amorphous silicon (a-Si:H) thin films.

[a]Permanent address: Departament de Física Aplicada i Electrònica, Universitat de Barcelona, Av. Diagonal 647, E-08028 Barcelona, Spain.

Downloaded 27 Sep 2010 to 161.116.168.227. Redistribution subject to AIP license or copyright; see http://rsi.aip.org/about/rights_and_permissions

II. OPTICAL FORMALISM

As already pointed out, FTPME combines the high-frequency modulation ($\omega = 37$ kHz) induced by a photoelastic device and the phase delay introduced by a Michelson interferometer (low frequency < 1 kHz) to record, in real time, the interferograms corresponding to the continuous, ω and 2ω frequencies. From these interferograms, the ellipsometric spectra corresponding to the quantities Ψ and Δ, defined by the complex reflectance ratio

$$\rho = \tan \Psi e^{i\Delta}, \quad (1)$$

can be obtained.

Let us recall that conventional FTIR spectrometers record the detected signal as a function of the optical path difference of two interfering beams, x. The detected intensity, $I(x)$, can be expressed by the following equation:[7]

$$I(x) = \int_0^\infty I(\sigma) \frac{1 + \cos 2\pi\sigma x}{2} d\sigma, \quad (2)$$

σ being the wave number defined as the inverse of the wavelength, $1/\lambda$. $I(\sigma)$ is the magnitude of the flux at that wave number and can be determined from the inverse FT of the interferogram $I(x)$.

The photoelastic modulator generates a periodic phase shift, $\delta(t)$, between the orthogonal amplitude components of the transmitted beam that, in the first-order approximation, is

$$\delta(t) = A_\sigma \sin \omega t, \quad (3)$$

where ω is the resonant angular frequency of the modulator unit and A_σ is the amplitude, which is a function of the peak-to-peak retardation of the photoelastic modulator.[14–16]

When coupling the interferometer to a dynamic photometric ellipsometer arrangement, the intensity displays a time modulation, that in the case of a phase-modulated ellipsometer with a polarizer-modulator-sample-analyzer configuration takes the form:[14]

$$\begin{aligned} I(\sigma,t) &= I[I_0 + I_c J_0(A_\sigma) + 2T_1 J_1(A_\sigma) I_s \sin \omega t \\ &\quad + 2T_2 J_2(A_\sigma) I_c \cos 2\omega t + ...] \\ &= S_0(\sigma) + S_\omega(\sigma) \sin \omega t + S_{2\omega}(\sigma) \cos 2\omega t + ..., \end{aligned} \quad (4)$$

where I depends on the overall setup transmission, I_0, I_s, and I_c are known functions of the ellipsometric angles Ψ and Δ and of the orientation of the optical components,[14] and $J_n(A_\sigma)$ is the nth Bessel function of the amplitude modulation, A_σ. I_0, I_s, I_c, and A_σ are functions of the wave number, whereas T_1 and T_2, which take into account the response of the detection system at frequencies ω and 2ω, respectively, are generally found independent of A_σ.[15,16]

Thus, combining Eqs. (2) and (4), the detected signal in FTPME takes the form:

$$\begin{aligned} I(x,t) = \int_0^\infty I(\sigma) \frac{1 + \cos 2\pi\sigma x}{2} [S_0(\sigma) + S_\omega(\sigma) \sin \omega t \\ + S_{2\omega}(\sigma) \cos 2\omega t]\, d\sigma. \end{aligned} \quad (5)$$

By calculating the dc, fundamental and second-harmonic components of the signal for each retardation, x, one can obtain the corresponding interferograms:

$$I_0(x) = \int_0^\infty I(\sigma) \frac{1 + \cos 2\pi\sigma x}{2} S_0(\sigma)\, d\sigma, \quad (6)$$

$$I_\omega(x) = \int_0^\infty I(\sigma) \frac{1 + \cos 2\pi\sigma x}{2} S_\omega(\sigma)\, d\sigma, \quad (7)$$

$$I_{2\omega}(x) = \int_0^\infty I(\sigma) \frac{1 + \cos 2\pi\sigma x}{2} S_{2\omega}(\sigma)\, d\sigma. \quad (8)$$

At this point, inverse FT allows the conversion of the interferograms into spectra:

$$I_0(\sigma) = I(\sigma) S_0(\sigma), \quad (9)$$

$$I_\omega(\sigma) = I(\sigma) S_\omega(\sigma), \quad (10)$$

$$I_{2\omega}(\sigma) = I(\sigma) S_{2\omega}(\sigma). \quad (11)$$

In order to determine the spectral dependence of the ellipsometric angles, the ratios R_ω and $R_{2\omega}$ are defined by

$$R_\omega = \frac{I_\omega(\sigma)}{I_0(\sigma)} = \frac{S_\omega(\sigma)}{S_0(\sigma)}, \quad (12)$$

$$R_{2\omega} = \frac{I_{2\omega}(\sigma)}{I_0(\sigma)} = \frac{S_{2\omega}(\sigma)}{S_0(\sigma)}. \quad (13)$$

The expressions of I_0, I_s, and I_c, that appear in Eq. (4), can be simplified by using a convenient orientation of the optical elements (polarizer, modulator, and analyzer).[14–16] The corresponding angles P, M, and A are referred to the plane of incidence. The most useful measurement configurations are: $P - M = \pm 45°$, $M = 0°$ $(+90°)$, $A = \pm 45°$, usually called configuration II, and $P - M = \pm 45°$, $M = \pm 45°$, $A = \pm 45°$, usually called configuration III. On the other hand, in phase-modulated ellipsometers with dispersive spectrometer the amplitude A_σ can be adjusted at each wave number in order to have $J_0(A_\sigma) = 0$; this also corresponds to large values of $J_1(A_\sigma)$ and $J_2(A_\sigma)$, resulting in very simple expressions of R_ω and $R_{2\omega}$.[14] The latter procedure cannot be used in FT ellipsometers, for which all the optical frequencies are detected at the same time and only one peak to peak retardation can be used [Eq. (3)]. This peak-to-peak retardation must be selected in such a way that the Bessel functions $J_1(A_\sigma)$ and $J_2(A_\sigma)$ lie near of their maximum value in the IR region of interest. The final expressions of R_ω and $R_{2\omega}$ are, in configuration II:

$$R_\omega = \pm \frac{2T_1 J_1(A_\sigma) \sin 2\Psi \sin \Delta}{1 \pm J_0(A_\sigma) \sin 2\Psi \cos \Delta}, \quad (14)$$

$$R_{2\omega} = \pm \frac{2T_2 J_2(A_\sigma) \sin 2\Psi \cos \Delta}{1 \pm J_0(A_\sigma) \sin 2\Psi \cos \Delta}, \quad (15)$$

and in configuration III:

$$R_\omega = \pm \frac{2T_1 J_1(A_\sigma) \sin 2\Psi \sin \Delta}{1 \pm J_0(A_\sigma) \cos 2\Psi}, \quad (16)$$

Downloaded 27 Sep 2010 to 161.116.168.227. Redistribution subject to AIP license or copyright; see http://rsi.aip.org/about/rights_and_permissions

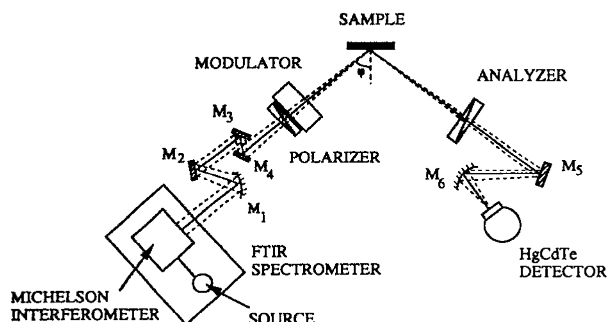

FIG. 1. Optical setup of the Fourier transform infrared phase modulated ellipsometer (FTPME).

$$R_{2\omega}=\pm\frac{2T_2 J_2(A_\sigma)\cos 2\Psi}{1\pm J_0(A_\sigma)\cos 2\Psi}, \tag{17}$$

from which the ellipsometric angles Ψ and Δ can be easily obtained. Finally, the ellipsometric measurements can be presented in the form of (Ψ,Δ), or using the complex optical density:[17]

$$D=\log\left(\frac{\rho_s}{\rho}\right)=\log\left(\frac{\tan\Psi_s}{\tan\Psi}\right)-i(\Delta-\Delta_s), \tag{18}$$

where ρ_s, Ψ_s is an example, and Δ_s refers to the substrate before film deposition. In the particular case of thin-film semiconductors deposited on glass, D is directly related to the complex dielectric function of the deposited film.[18]

III. DESCRIPTION OF THE ELLIPSOMETER

The FTPME consists of an optical setup and a data acquisition system that provides the spectral dependence of the angles Ψ and Δ of the sample.

A. Optical setup

The optical setup of the ellipsometer is schematically shown in Fig. 1. The sample under measurement is placed between two optical benches on the incident and reflected beam sides. The optical bench on the incident beam side consists of a light glowbar source, a Michelson interferometer, a focusing optical system, a polarizer, and the photoelastic modulator. On the reflected beam side the optical bench includes an analyzer, a focusing optical system, and a detector. The modulator and the analyzer are mounted on 1′ precision automatic rotators. A 15′ precision rotator mounted on the modulator allows orientation of the polarizer at an angle corresponding to $P-M=\pm 45°$. The angle of incidence is fixed at about 70°.

A commercial IR spectrometer (BOMEM-MB100), placed on the incident beam, includes a glowbar source which consists of a silicon carbide rod heated at 1100 K. The Michelson interferometer provides a parallel IR light beam of 38 mm diameter. This beam is focused within an area of 1 cm^2 on the sample surface by means of four mirrors: an off-axis paraboloidal (M_1), a flat (M_2), and two spherical concave (M_3, M_4) mirrors. Before reaching the sample, the IR beam passes through the IR grid polarizer and the photoelastic modulator (Hinds–Morvue PEM-80). The latter consists of an octagonal block of ZnSe cemented on a piezoelectric quartz crystal oscillating at a frequency of $\omega=37$ kHz. After the sample reflection, the beam passes through the analyzer (IR grid polarizer) and is focused onto the sensitive area, namely, 1 mm^2, of a nitrogen-cooled photovoltaic HgCdTe detector (MCT). The focusing system is constituted by spherical concave (M_5) and off-axis paraboloidal (M_6) mirrors.

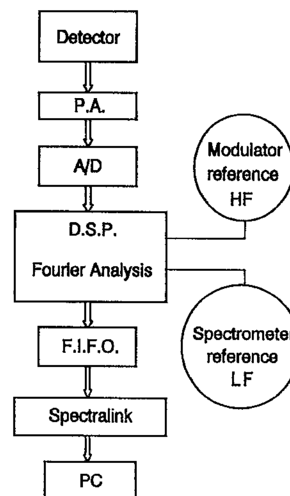

FIG. 2. Diagram of the data acquisition system.

The IR grid polarizers used present losses of about 1%. This affects the operation procedure in the way that we can only work in the first-order approximation of the optical formalism [Eq. (3)]. With perfect polarizers we can use the same formalism as in the visible-UV,[15] and the accuracy will be improved. In this way, new polarizers will be adapted.[19]

The accessible domain of wave numbers, restricted by the detector specification, ranges from 900 to 4000 cm^{-1}. Moreover, the performance of the modulator allows its extension from 500 to 18000 cm^{-1}. The resolution which varies inversely as the maximum optical path difference can be varied from 1 to 128 cm^{-1}. All the spectra presented in this article were recorded at a resolution of 4 cm^{-1}.

All the optical elements, including the sample, are enclosed in sealed boxes. A dry nitrogen flow is introduced in the boxes in order to purge water and carbon dioxide.

B. Data acquisition system

The schematic diagram of the data acquisition system is displayed in Fig. 2. The electrical signal provided by the MCT detector is preamplified and transmitted to the readout system which is connected to a computer through a multi-instrument modular package (Spectralink of ISA Jobin Yvon). The read out system basically consists of a gain-controlled amplifier, a high-precision fast ADC (16 bits, 500 kHz), a digital signal processor (DSP Motorola 56001) and a first-in–first-out register (FIFO). The gain-controlled amplifier is dedicated to obtain a good fit between the preamplified signal and the ADC input range in

Downloaded 27 Sep 2010 to 161.116.168.227. Redistribution subject to AIP license or copyright; see http://rsi.aip.org/about/rights_and_permissions

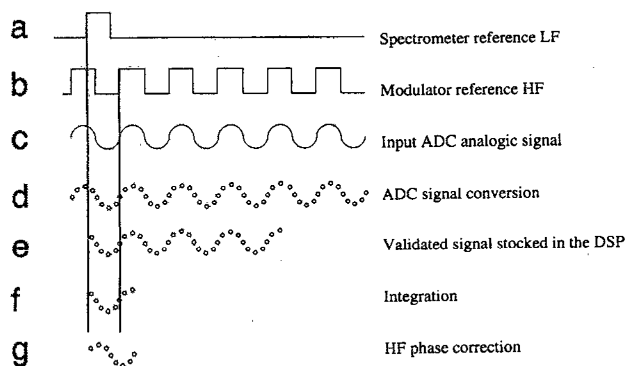

FIG. 3. Synchronization operation.

order to reduce quantization noise. The digital signal processor controls the data acquisition by synchronizing the ADC conversions with the displacement of the Michelson interferometer. The DSP also carries out the Fourier analysis of the ω signal [see Eq. (5)] and transfers the result (dc, fundamental, and first-harmonic components) to the FIFO register where it is accumulated. This register is read in real time by a computer through the Spectralink network.

An interferogram is composed of 2^n signal measurements recorded at equal increments of optical path difference. Commercial FTIR spectrometers incorporate an internal He–Ne laser in order to obtain a sinusoidal interferogram that yields the optical path difference feedback. In those instruments the analog-to-digital conversion is triggered at the zero crossing of the laser fringe signal. In the ellipsometric configuration presented here, the analog-to-digital conversion must be synchronized with two signals: the laser fringe interference signal of the spectrometer and the ω reference signal of the modulator. Figure 3 illustrates the synchronization procedure. On the top of the figure the spectrometer low-frequency (a) and the modulator high-frequency (b) references are shown. The ADC performs continuously the signal conversion (c,d) which most of the time is not validated, that is, the result of the conversion is not read by the DSP. When the DSP detects a laser fringe interference, signal conversion is validated and the sampled points are stocked in the DSP internal memory (e). The acquisition cycle of one signal measurement consists of the accumulation of four successive periods of the signal (e), each period being sampled in 8 points. That is, for every laser signal the ADC performs 32 consecutive conversions corresponding to four periods of the ω signal. Then a digital integration of the four stocked periods is performed (f). The stored signal (f) is not in phase with the modulator reference (b) and a rearrangement of the eight points is necessary in order to maintain the phase. The rearrangement is easily accomplished by, first, counting the number of sampled points, n, between the laser reference signal and the modulator reference signal (in the figure, the number of points between the solid lines) and, second, by shifting n times the points after integration. Thus, the first point in the final stocked signal (g) will be in phase with the modulator reference.

Since the reflector drive of the spectrometer is continuous, the optical path difference will not remain constant during the acquisition of four consecutive periods and, therefore, a phase error will be introduced in the interferogram. To reduce this error the reflector scanning speed has been decreased from its nominal value of 2 to 0.660 mm/s, leading to a laser fringe interference frequency of 2.116 kHz. Within this condition there are 17.5 periods of $\omega = 37$ kHz between two laser signals. Phase error would be improved by further decreasing the scanning speed or by decreasing the number of accumulations. However, such a decrease would deteriorate real time performances and signal-to-noise ratio.

C. Data reduction

Data reduction follows the signal Fourier analysis performed by the DSP. The results are transferred to the computer through the FIFO register, and are stored in real time into the computer RAM memory. When the data acquisition is finished, the data are rearranged by the computer in form of dc, fundamental, and first-harmonic interferograms. At this point, in order to improve the signal-to-noise ratio, interferogram accumulation can be performed. Then, each interferogram is transformed into its respective spectrum by means of the FFT algorithm [Eqs. (6)–(8)], which allows the calculation of the ratios $R_\omega(\sigma)$ and $R_{2\omega}(\sigma)$, defined by Eqs. (12) and (13). Finally, the ellipsometric angles are obtained and thus the complex quantities ρ and D defined in the Eqs. (1) and (18).

Full spectra can be taken in 2 s but the precision of the angles Ψ, Δ is improved from 0.3° to 0.02° when the time of the accumulation of spectra increases from 2 to 760 s. However, it has to be pointed out that the precision depends on the absolute values of Ψ and Δ.

IV. CALIBRATION

A. Orientation

The first step of the orientation of the optical components deals with the alignment of the polarizer, modulator, sample, and analyzer assembly that is accomplished with the help of a He–Ne laser; afterwards, the IR source and detector are added and the whole alignment is performed with the use of a digital oscilloscope. This operation consists on optimizing the detected intensity by tuning the optical system. The next step consists of the determination of the reference position for each optical element that must be achieved by using a nontransparent sample ($\Delta \neq 0°$). In this way, the signal has nonzero fundamental and second-harmonic components in the more general case of orientation. To obtain $M-P=0°$ or 90° the polarizer has to be rotated until both modulated components vanish for every modulator or analyzer orientations. The polarizer is then rotated to $\pm 45°$ from the obtained reference position to have $M-P=\pm 45°$. In this situation, the reference orientations $A=0°$ and $M=0°$ are determined by minimizing the fundamental harmonic component proportional to sin 2A and the first-harmonic component proportional to sin $2M$, respectively.[14,15]

Downloaded 27 Sep 2010 to 161.116.168.227. Redistribution subject to AIP license or copyright; see http://rsi.aip.org/about/rights_and_permissions

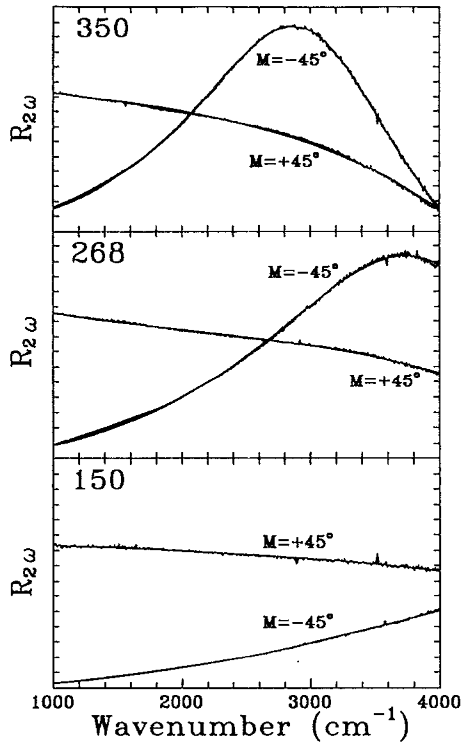

FIG. 4. Calibration figures corresponding to the experimental and fit functions of the $R_{2\omega}$ spectra, at $M=\pm 45°$, for three tensions of the modulator: 150, 268, and 350 (in arbitrary units).

B. Bessel functions background

The dependence of the modulation amplitude A_σ on the wave number produces a Bessel function background in the obtained spectra [see Eq. (4)]. When studying a given IR frequency region care must be kept to adjust the drive voltage of the photoelastic modulator to have a small value of $J_0(A_\sigma)$ and, consequently, $J_1(A_\sigma)$, and $J_2(A_\sigma)$ near its maximum values. In the most general case, when studying the whole IR region accessible to the ellipsometer (900–4000 cm^{-1}), the peak-to-peak retardation is fixed to 2.671 μm. In this condition the minimum value of A_σ is 0.815 rad and the maximum 3.62 rad; therefore $J_1(A_\sigma)$ takes values between 0.08 and 0.374 and $J_2(A_\sigma)$ between 0.078 and 0.44. The calibration procedure of A_σ will be described in Sec. IV C 1.

C. Frequency response

The determination of the response coefficients, T_1 and T_2, can be summarized in the following four step process:

1. Determination of T_2

We use the orientation $P-M=\pm 45°$, $A=0°$, $M=\pm 45°$ in which the ratio $R_{2\omega}$ takes the form:

$$R_{2\omega}=\frac{2T_2 J_2(A_\sigma)}{[1\pm J_0(A_\sigma)]}. \qquad (19)$$

One can then compute T_2 by fitting the measured $R_{2\omega}$ spectrum using a least-squares method and taking T_2 and $K=A_\sigma/\sigma$ as parameters. Figure 4 shows the calibration curves corresponding to three different tensions of the modulator: 150, 268, and 350 (in arbitrary units). Each one presents the experimental measured values of $R_{2\omega}$, recorded at two angular positions of the modulator ($\pm 45°$) and the fitted functions. Figure 4 shows that a very good fit is attained. The values obtained for T_2 were 0.84, 0.89, and 0.92, as the tension increased. In the same range of variation, K_σ had the values: 6.6×10^{-4}, 9.3×10^{-4}, and 1.2×10^{-3}.

2. Determination of Ψ

We use the orientation $P-M=\pm 45°$, $A=\pm 45°$, $M=\pm 45°$ in which the detected intensities take the form:[14–16]

$$I_0=1$$
$$I_s=\pm\sin 2\Psi \sin\Delta, \qquad (20)$$
$$I_c=\pm\cos 2\Psi$$

therefore

$$R_{2\omega}=\frac{2T_2 J_2(A_\sigma)I_c}{[1\pm J_0(A_\sigma)I_c]} \qquad (21)$$

and

$$\Psi=\frac{1}{2}\cos^{-1}\left(\frac{\pm R_{2\omega}}{2T_2 J_2(A_\sigma)-R_{2\omega}J_0(A_\sigma)}\right). \qquad (22)$$

3. Determination of Δ

We use the orientation $P-M=\pm 45°$, $A=\pm 45°$, $M=90°$ or $0°$ in which the detected intensities take the form:

$$I_0=1$$
$$I_s=\pm\sin 2\Psi \sin\Delta. \qquad (23)$$
$$I_c=\pm\sin 2\Psi\cos\Delta$$

The expression of $R_{2\omega}$ is the same as above [Eq. (21)] and

$$\Delta=\cos^{-1}\left(\frac{\pm R_{2\omega}}{2T_2 J_2(A_\sigma)-R_{2\omega}J_0(A_\sigma)}\frac{1}{\sin 2\Psi}\right). \qquad (24)$$

4. Determination of T_1

We use the same orientation as in step 2, in which the expression of R_ω is

$$R_\omega=\frac{2T_1 J_1(A_\sigma)I_s}{[1\pm J_0(A_\sigma)I_c]}, \qquad (25)$$

therefore:

$$T_1=\frac{[1\pm J_0(A_\sigma)I_c]R_\omega}{2J_1(A_\sigma)I_s}. \qquad (26)$$

Once Ψ and Δ are known, T_1 can be calculated and takes a nearly constant value of 0.85 independent of the wavelength.

Downloaded 27 Sep 2010 to 161.116.168.227. Redistribution subject to AIP license or copyright; see http://rsi.aip.org/about/rights_and_permissions

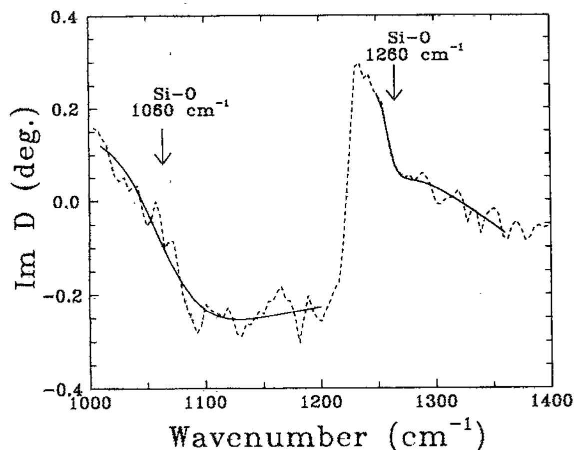

FIG. 5. Imaginary part of the optical density D for a crystalline silicon sample (c-Si), with an overlayer of 20 Å of native oxide (dotted line), fitted assuming two Lorentzian behaviors (solid lines). The optical density is referred to the c-Si etched substrate.

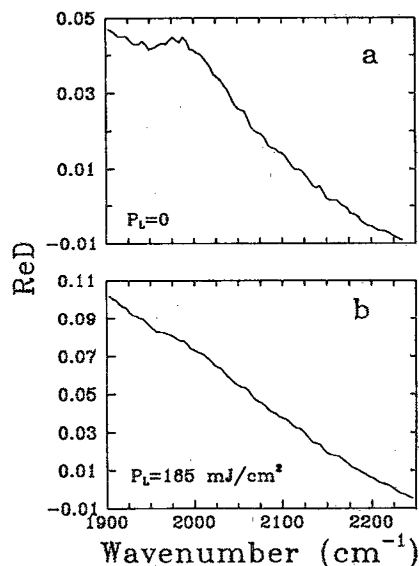

FIG. 6. FTPME spectrum (Si–H stretching mode region) of the optical density Real part, ReD, of two samples of hydrogenated silicon thin films (400 Å): (a) amorphous, (b) crystallized silicon obtained by applying an UV laser power of 165 mJ/cm^2 during growth.

V. EXAMPLES OF APPLICATION

This FTPME has been used in several studies of different materials and structures. For example, the study of thin films of Pt-Al_2O_3 cermets,[20] and the study of the adhesion of dielectric thin films on polymer substrates.[21] Two examples of application are presented to illustrate the measurement sensitivity. It has to be noticed that the noise level in Ψ and Δ is very weak ($\sim$0.03°) as compared to the 1° level obtained with conventional IRPME using the same IR source and detector.[22] To reach this level, FTPME needs an integration time for full spectrum of 380 s (1240 points) in contrast of IRPME with a cascade arc source which needs an integration time of 10 s/point.

A. Native oxide film on c-Si

A sample of c-Si was etched by a diluted solution of HF (10%) in order to eliminate the native oxide overlayer, whose thickness is generally estimated around 20 Å. Spectra were taken before and after etching, keeping the samples in an atmosphere of dry nitrogen. The optical density D [defined by the Eq. (18)] is referred to the clean c-Si as a substrate. In Fig. 5, the dispersive behavior of the imaginary part of D, in the spectral range from 1000 to 1400 cm^{-1}, is shown (dashed line). Two Si–O bond-stretching vibrations, which correspond to the transverse and longitudinal absorptions of SiO_2,[11,23,24] were clearly identified in this range. In contrast with IR reflection spectroscopy, IR ellipsometry does not require the use of multiple internal reflections[25] to achieve enough sensitivity to identify in this overlayer the two absorption peaks. A good fit was obtained with a Lorentzian behavior (solid lines) for each one and they were associated to the lines centered at $\omega_{01}=1060$ cm^{-1} and $\omega_{02}=1260$ cm^{-1}.

B. Amorphous silicon crystallization

The crystallization process during film growth influences the hydrogen incorporation in hydrogenated amorphous silicon (a-Si:H) thin films. The crystallization of a-Si:H thin films, 400 Å thick, was achieved by applying an ultraviolet (UV) light emitted by a XeCl excimer laser, simultaneously with the plasma-enhanced chemical vapor deposition, from silane gas, on glass substrates kept at 250 °C.[26] The films obtained without UV radiation contain about 15% hydrogen. By increasing the laser power, the evolution from amorphous to polycrystalline material is observed, and for a laser power of 165 mJ/cm^2 the characteristic peaks, at 3.4 and 4.2 eV, of crystallized silicon appear in the spectra of imaginary part of the dielectric constant.

FTPME allows the study of the hydrogen incorporation in these a-Si:H thin films. Full FTPME spectra were obtained by integrating during 380 s, in order to obtain a resolution on Ψ and Δ of 0.03°. Figures 6 and 7 correspond to the spectra, in the Si–H stretching modes range, of the real (ReD) and imaginary part (ImD) of D [Eq. (18)], respectively. The sample obtained without laser radiation (a) shows a clear maximum of ReD at 2000 cm^{-1}, which corresponds to a change in the slope of ImD, associated to the SiH bond. For the crystallized sample (b), this contribution almost vanishes. This evolution can be associated to the decrease of the hydrogen bonded as SiH.

VI. SUMMARY AND CONCLUSION

We have described a new FTIR phase-modulation ellipsometer (FTPME). The coupling between low-frequency FTIR spectroscopy and high frequency of phase modulation ellipsometry is obtained by means of an original data acquisition system, which is based on a digital microprocessor (DSP) well adapted to the FFT. A self-consistent spectral procedure has been presented. It allows to record a spectrum from 900 to 4000 cm^{-1} in 2 s, with 4 cm^{-1} of resolution. The precision on Ψ and Δ can reach

Downloaded 27 Sep 2010 to 161.116.168.227. Redistribution subject to AIP license or copyright; see http://rsi.aip.org/about/rights_and_permissions

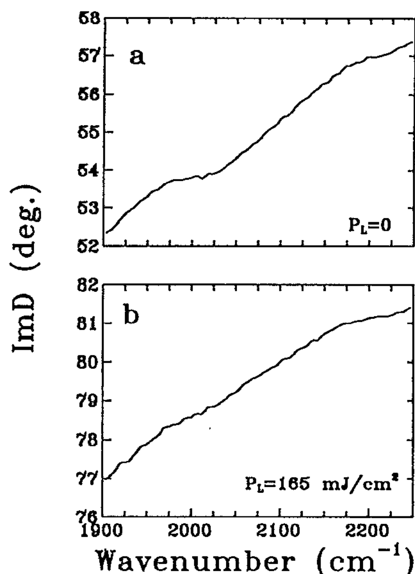

FIG. 7. FTPME spectrum (Si–H stretching mode region) of the optical density Imaginary part, ImD, of two samples of hydrogenated silicon thin films (400 Å): (a) amorphous, (b) crystallized silicon obtained by applying an UV laser power of 165 mJ/cm^2 during growth.

0.02° for integration time of 750 s. The high sensitivity of this technique (a few angstroms) has been revealed by two examples.

In conclusion, the FTPME appears as a powerful technique to perform detailed analyses in real time of the vibrational properties of surfaces and interfaces.

ACKNOWLEDGMENTS

The authors are grateful to J. Huc and J. Y. Parey for technical assistance. Helpful discussions with R. Benferhat, A. Darier, and Y. Josserand of ISA Jobin Yvon were greatly appreciated. The authors also thank the financial support from the Agence Nationale pour la Valorisation de la Recherche (ANVAR). One of the authors (E.P.) acknowledges a grant from the Ministère de la Recherche et de la Technologie (France).

[1] R. W. Stobie, B. Rao, and M. J. Dignam, Appl. Opt. **14**, 999 (1975).
[2] A. M. Bradshaw and F. M. Hoffmann, Suf. Sci. **72**, 513 (1978).
[3] R. Benferhat, B. Drévillon, and P. Robin, Thin Solid Films **156**, 295 (1988).
[4] A. T. M. Wilbers, G. M. W. Kroesen, C. J. Timmermans, and D. C. Schram, Meas. Sci. Technol. **1**, 1326 (1990).
[5] N. Blayo, B. Drévillon, and R. Ossikovski, SPIE Symp. Proc. **1681**, 116 (1992).
[6] N. Blayo and B. Drévillon, Surf. Sci. **260**, 37 (1992).
[7] R. J. Bell, *Introductory Fourier Transform Spectroscopy* (Academic, New York, 1972).
[8] A. Röseler, Infrared Phys. **21**, 349 (1981).
[9] F. Ferrieu, Rev. Sci. Instrum. **60**, 3212 (1989).
[10] J. Bremer. O. Hunderi, K. Fanping, T. Skauli, and E. Wold, Appl. Opt. **31**, 471 (1988).
[11] K. B. Koller, W. A. Schmidt, and J. E. Butler, J. Appl. Phys. **64**, 4704 (1988).
[12] R. T. Graf, F. Eng, J. L. Koening, and H. Ishida, Appl. Spectrosc. **40**, 498 (1986).
[13] B. Dévillon and A. Canillas, French patent, No. 9200090 (1992).
[14] S. N. Jasperson and S. E. Schnatterly, Rev. Sci. Instrum. **40**, 761 (1969).
[15] O. Acher, E. Bigan, and B. Drévillon, Rev. Sci. Instrum. **60**, 65 (1989).
[16] B. Drévillon, J. Perrin, R. Marbot, A. Violet, and J. L. Dalby, Rev. Sci. Instrum. **53**, 969 (1982).
[17] M. J. Dignam and J. E. Fedyck, Appl. Spec. Rev. **14**, 249 (1978).
[18] B. Drévillon and R. Benferhat, J. Appl. Phys. **63**, 5088 (1988).
[19] K.-L. Barth, D. Böhme, K. Kamaras, and F. Keilmann, Proceedings of the First International Conference on Spectroscopic Ellipsometry, Paris (France) 1993.
[20] J. P. Segaud, B. Drévillon, E. Pascual, R. Ossikovski, G. Monnier, and L. Rimbourg, Thin Solid Films (in press).
[21] S. Vallon, B. Drévillon, and J. C. Rostaing, Thin Solid Films (in press).
[22] N. Blayo and B. Drévillon, Appl. Phys. Lett. **57**, 786 (1990).
[23] F. Ferrieu and J. H. Lecat, J. Electrochem. Soc. **137**, 2203 (1990).
[24] J. E. Olsen and F. Shimura, Appl. Phys. Lett. **53**, 1934 (1988).
[25] F. Müller, N. Schwarz, V. Petrova-Koch, and F. Koch, Appl. Surf. Sci. **39**, 127 (1989).
[26] N. Layadi, P. Roca i Cabarrocas, V. Yakovlev, and B. Drévillon, Appl. Surf. Sci. **69**, 262 (1993).

Downloaded 27 Sep 2010 to 161.116.168.227. Redistribution subject to AIP license or copyright; see http://rsi.aip.org/about/rights_and_permissions